Numerical study on stainless steel I-shaped links on eccentrically braced frames

R. Chacón, A. Vega, E. Mirambell
Department of Civil and Environmental Engineering
Universitat Politècnica de Catalunya

Abstract

Strength, ductility and strain-hardening on austenitic stainless steel are interesting structural properties that suggest a potential strategic structural application as dissipative members in seismic-resistant systems. Eccentrically braced frames (EBF) are structural systems that dissipate energy during seismic episode by means of shear- or bending-shear related mechanisms in particular elements commonly referred to as links. The use of austenitic stainless steel in these links may represent an interesting alternative for EBF. As a strategic solution aimed at exploiting the stainless steel structural properties, non-dissipative zones may be assembled with carbon steel whereas dissipative zones may be assembled with austenitic stainless steel. This paper presents a numerical study on austenitic stainless steel, I-shaped, short links on EBF subjected to cyclic loading. The study encompasses a set of parametric analysis in which the web slenderness, transverse stiffening and material properties of the elements are systematically varied. Strain-hardening, energy dissipation and residual displacement are evaluated for stainless steel links and the carbon steel counterparts. The results suggest that austenitic stainless steel links may provide to the EBF system an interesting solution that enhances their overall behaviour during energy dissipation-related episodes.

Keywords: Structural links, Eccentrically braced frames, Austenitic stainless steel

1. Introduction

Eccentrically braced frames (EBF) are a widely accepted form of seismic force resisting system (or more broadly, of all kinds of lateral forces). These structures were firstly reported in Japan [1,2] during the seventies as a seismic resisting system with both high elastic stiffness and high energy dissipation. EBF are systems in which the braces are connected to relatively short beams or columns instead of to a node of the structure. These short segments are commonly referred to as links. Different geometrical configurations of EBF can be found in routinely designed seismic resisting steel structures in which links happen to be horizontal, vertical, centred or laterally placed. Figure 1 shows an isometric view of a spatial EBF system with provided horizontal links in two-resisting directions.

EBF systems are generally designed in such a way that during seismic episodes, failure is concentrated in these links, which act as structural fuses. These elements may be subjected to cyclic loads that may result in considerable plastic strains. The length of a link segment "e" controls its overall structural behaviour as well as the behaviour of the whole EBF system. One parameter that has been used for characterising the overall behaviour of the links is the length ratio $\rho=e/(M_p/V_p)$, in which M_p is the plastic moment and V_p are plastic shear capacity of the element. Generally speaking, these links may be designed as short, resulting in energy dissipation with shear-related mechanisms or as medium- to long, resulting in energy dissipation with shear-bending or bending-related failure modes. Some authors [3,4] have found that links with a ratio $\rho \leq 1.6$ may be considered as short whereas intermediate- to longs links present a ratio $\rho > 1.6$. In terms of strength and ductility, research suggest that short links subjected to cyclic loading perform better than the long counterparts do. The structural analysis of EBF and links have been an active research line in the U.S that has contributed to the continuous update to the design codes [5-8].

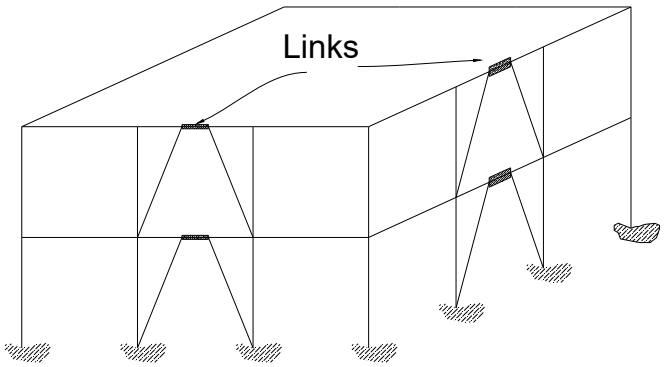

Fig. 1 EBF spatial systems with horizontal links

On the other hand, the use of stainless steel in structures has increased in recent years due to its unique combination of mechanical properties, durability and aesthetics [9]. The mechanical properties of stainless steel such as ductility, toughness, considerable strain-hardening and good fire resistance make it a quite suitable material for structures required to withstand accidental loading due to seismic and/or fire events. Links are conceived as structural fuses, experiencing inelastic rotation while other components remain essentially elastic. Therefore, short links in stainless steel may represent a strategic solution in which their structural properties are related to ductility and strain-hardening are exploited considerably. Hybrid structures with stainless steel in dissipative zones and carbon steel in non-dissipative zones may represent a solution leading to several beneficial aspects for the whole system. The energy-dissipation mechanisms are enhanced due to greater strain-hardening and greater ductility, which allow designing non-dissipative zones more efficiently. However, since non-dissipative zones are meant to remain essentially elastic, careful consideration of excessive strain-hardening of the links needs to be addressed.

This paper provides a numerical study in which I-shaped stainless steel short links with varying material and geometrical configurations are analysed when subjected to cyclic loading. The study is focused on members belonging to EBF systems that are modelled as isolated members by adopting realistic boundary conditions. Shell-based analysis of such members is performed by including geometrical and material nonlinearities considering imperfections (GMNIA). The results obtained provide comparisons in terms of energy-dissipation, ductility and overall strength of both stainless- and carbon steel links subjected to cyclic loading.

2. Literature review

2.1 Structural links in eccentrically braced frames

Links on carbon steel EBF have actively been studied in recent years. Short links subjected to cyclic loading have been a matter of study in last decades via analytical research. Predicting models aimed at providing the cyclic response of short and long links including partially or fully isotropic and kinematic hardening are available [10-13]. Likewise, several experimental programs in which EBF with different configurations are reported in the literature. Tests with I-shaped configurations [14-16], tubular elements [17], high-strength steel links [18], replaceable elements [19-21], vertical Y-links [22-25] (which possess the advantages of horizontal links but add a certain ease of dismantling in medium- to long elements) and retrofitting or forensics post-quake engineering can be found [26-27]. A recently published comprehensive state-of-the-art review including characteristics, detailing and description of EBF systems includes a vast selection of references and identifies key aspects related to research and design [28]. In this review, it is pinpointed that newly proposed concepts such as composite links, EBFs with shape

memory alloy (SMA) devices, EBFs made of high strength or stainless steel are potential areas for studies due to several reasons such as increasing ductility and energy dissipation in nonlinear metallic materials. Both American AISC [29] and European provisions EN1998 [30] provide design basis for the verification of steel links. In both cases, links are classified as short, intermediate or long by defining limits of the link length ratio. Table 1 displays such limits, as well as: the shear resistance V_p, the flexural resistance M_p and the maximum rotation of the links. Small variations in such values as well as in the conceptual design of these members are observed. The intermediate- to long links limits are slightly different as well as the definition of the plastic bending resistance of the segments (full plastic resistance according to [29], plastic resistance of the flanges only according to [30]). Particularly, assessment of the importance of link models when evaluating the response of frames designed with EN1998 are depicted in [23,31].

	ANSI/AISC (2016) [22]	EN1998 (2004) [23]
Limits	$\rho \leq 1.6$ short links $1.6 \leq \rho \leq 2.6$ intermediate links $\rho \geq 2.6$ long links	$\rho \leq 1.6$ short links $1.6 \leq \rho \leq 3.0$ intermediate links $\rho \geq 3.0$ long links
Shear resistance	$\phi_v \cdot V_p = 0.90 \cdot \left[0.6 \cdot F_y \cdot \left(d - 2 \cdot t_f \right) \cdot t_w \right]$	$V_{p,link} = \left[0.6 \cdot f_y \cdot \left(d - t_f \right) \cdot t_w \right] / \sqrt{3}$
Flexural resistance	$M_p = Z \cdot F_y$ Being Z the plastic modulus	$M_{p,link} = b \cdot t_f \cdot f_y \cdot \left(d - t_f \right)$
Maximum allowable rotation	0.08 rad	0.08 rad

Table 1. Links structural characteristics according to AISC [22] and EN1998 [23]

Based on empirical experiences, one of the fundamental aspects that has been pinpointed in short steel links is that these elements can exhibit three different modes of behaviour: Elastic, Inelastic pre-buckling and post-buckling [4]. These three modes are related to three states: yielding, buckling and failure. Researchers have presented attempts to quantify these states for the sake of appropriately designing active links [4] [32]. These states must be particularly addressed in the case of nonlinear metallic alloys (such as stainless steel or aluminium) in which transitions between these states may be specially blurred. Studies related to the behaviour of aluminium [33] and stainless steel links [34] are available. In the study related to stainless steel links [34], quasi-static nonlinear numerical simulations were performed following the incremental protocol suggested in AISC provisions. Noticeably, this protocol is based on applying cycles that are increased from one to another until failure.

2.2 Cyclic loading in stainless steel

Stainless steel is a metal alloy resulting from the mixture of mostly iron and a minimum of 10.5% chromium. When exposed to oxygen, the chromium forms a self-repairing chromium-rich thin oxide surface, protecting the steel from additional interaction with an oxidizing agent and hence, stainless steel becomes a highly attractive structural material that overcomes one of the weaknesses of carbon steel, i.e. corrosion.

Unlike carbon steel, stainless steels have a rounded stress-strain curve with no plateau and with no well-defined yield point. Another significant difference between these materials is that stainless steel exhibits a considerable strain hardening and high ductility; this means that it is able to absorb impact without fracturing and it reaches strains of 40-60% at fracture when monotonically loaded. Furthermore, stainless steels present anisotropic as well as non-symmetric behavior. The yield strength in non-linear materials such as stainless steel is generally determined as a proof strength for a particular offset permanent strain; in the case of stainless steel, the yield strength is conventionally established as the proof strength for a 0.2% offset strain. In last decades, several material models have been developed to analytically reproduce the stainless steel behavior [35-37]. These models are built from a set of parameters obtained from experimental tests aimed at providing an accurate representation of the material behavior accounting for its nonlinearity.

When it comes to describing the stainless steel cyclic behavior, a material model capable of simulating accurately its cyclic material properties (such as the Bauschinger effect as well as the expansion of the yield surface) is needed. In previous studies [38-41], the defining characteristics of the strain hardening of the material are derived from a combined isotropic/kinematic hardening rule based upon the Chaboche model [42], which proves adequate to fulfill these criteria.

The model consists of a combined representation of isotropic and kinematic hardening. The isotropic hardening behavior defines the evolution of the yield surface size (σ^0), as a function of the equivalent plastic strain (ε^p). Eq. (1) shows this relationship in which $\sigma|_0$ is the yield stress at zero plastic strain (defined in this study as 0.2% proof stress), Q_∞ is the maximum change in the size of the yield surface and b is a parameter that defines the rate at which the size of the yield surface changes as plastic strain increases.

$$\sigma = \sigma|_0 + Q_\infty \cdot \left(1 - e^{-b\varepsilon_p}\right) \tag{1}$$

The change of backstress α is defined according to the kinematic component of the model shown in Eq. (2), where C_k is the initial kinematic hardening modulus and γ_k is the rate at which the kinematic hardening modulus decreases with increasing plastic deformation. The ratio C_k/γ_k is known as the maximum variation in backstresses. A backstress is the stress coordinate of a point midway between the yield stress in tension and the yield stress in compression.

$$\alpha = \frac{C_k}{\gamma_k} \cdot \left(1 - e^{-\gamma\varepsilon^p}\right) + \alpha_1 e^{-\gamma\varepsilon^p} \tag{2}$$

It is important to point out that this calibration is developed from tests in which a set of loading-unloading cycles is performed. Desirably, hysteresis strain cycles at constant strain need to be performed until the material stabilizes. Stabilization is defined when in subsequent cycles of identical strain amplitude, the measured maximum stress is asymptotically constant.

On the other hand, as expected, the number of cycles at which fracture occurs in tests decrease with the applied strain. Attempts for calibration of Coffin-Manson curves for stainless steel subjected to cyclic loading for low cycle fatigue LCF and extremely low fatigue ELCF have been reported [38]. These authors fitted experimental data including cold-worked and hot-rolled specimens. Similarly to other alloys, when stainless steel is cyclically subjected to strain at high levels, the number of cycles at which fracture occurs decrease drastically.

2.3 Shear in stainless steel elements

Stainless steel members have been increasingly used for structural applications in recent years due to high corrosion resistance, ease of maintenance, aesthetics and improved fire resistance. Although the basis of design of stainless steel structures are fundamentally similar to those for carbon steel, different specification procedures or calibrations of design expressions are often encountered in relevant guidelines and design manuals [43-45]. Applications of stainless steel in construction date back about 90 years and include landmark examples. Hot-rolled, cold-formed and built-up stainless steel members have been studied when subjected to various types of loading and geometrical configurations [46]. The particular case of stainless steel elements subjected to predominantly static shear loads has been studied in recent years in plate girders [47-51]. These studies have been based upon experimental programs and numerical investigations on plate girders assembled primarily with slender web panels. A systematic evaluation and calibration of the mechanical models [52-54] that depict the shear buckling response of steel plate girders is addressed in [47]. More than thirty experimental tests on stainless steel plate girders subjected to shear were used in this appraisal. European guidelines [43] [55] as well as the model provided by Estrada et al. in [56] were assessed. Revised expressions of the web buckling coefficients were proposed with a corresponding reliability analysis.

A fundamental conclusion of all studies related to shear in stainless steel girders is the analogy of the shear response with the one observed in carbon steel girders. In plate girders with slender web panels under shear loading, the web panels buckle firstly. Subsequently, a post-buckling tension field action occurs and eventually, a multi-hinge frame mechanism defines the ultimate load of these elements. Depending on the web slenderness as well as the transverse and longitudinal stiffening, the material non-linearity influences this response to a certain extent. Nevertheless, less research is available for the case of hot-rolled stocky elements subjected to shear.

2.4 Stainless steel structures subjected to seismic loading.

Research related to stainless steel structures subjected to arbitrary cyclic loading is not profuse. One of the first investigations that can be found in the literature was presented by DiSarno et al. [57]. Stainless steel frames (as well as their corresponding carbon steel ones) were studied numerically under cyclic loading with finite beam-element models. The cyclic properties of stainless steel were introduced based upon previously reported results. A set of fifty frames with varying geometrical and material configurations were simulated under pushover analysis as well as under dynamic response history. Global parameters such as the base shear, inter-storey drifts, energy absorption capacity and redistribution potential were assessed. Stainless steel frames were found interesting for the design of earthquake-resistant frames under certain design considerations such as: regularity, the density of stainless steel members and its strategic use in structural fuses throughout the frame. In 2008, the same authors published research findings [58] related to the use of stainless steel braces in dissipative zones of concentric (CBF) and eccentric (EBF) frames by assessing a set of regular multi-storey buildings previously designed in compliance with capacity-design rules. Carbon steel frames were set as benchmark and comparisons between different material variations were performed. FE-based simulations were performed and extensive inelastic static and dynamic analyses were carried out. Stainless steel frames showed enhanced properties when used in these systems after analyzing plastic deformations and the energy absorbing capacity. Strain-hardening was found particularly beneficial in the frames that included stainless steel in the dissipative zones and plastic strain was found to be more spread throughout these members.

More recently, by using detailed shell-based FE-simulations, a series of comparisons between different link configurations in EBF were presented in [59]. Different alloys (carbon, austenitic and ferritic stainless steels) were investigated under conservative assumptions of limited strain hardening enhancement of the material when subjected to cyclic loading. Those preliminary results pinpointed key aspects of the structural response of short links in EBF such as the influence of the stiffening as well as of the material variation. Subsequent investigations with updated analysis of the strain-hardening enhancement of austenitic stainless steel have been included [60]. Strategic use of stainless steel elements as tubular braces in CBF has been investigated in [61]. Experimental investigations on specimens with varying global and local slenderness were presented. Tensile ductility was observed in specimens with compact sections and local buckling was only observed in very slender cross-sections. Energy dissipation was also dependent on the compactness of the members. Similarly to other results related to cyclic plasticity in stainless steel, the fracture life of the specimens was perceived as dependent on the loading history.

3. Numerical study

A numerical study on I-shaped stainless- and carbon steel links was performed. The study was developed on isolated elements corresponding to links in EBF subjected to cyclic loading. Extended information related to these geometries as well as to other types of cross-sections and full-scale reproductions of EBF are also included in [62]. A numerical model implemented in Abaqus-Simulia [63] was used as a simulation tool. Fully non-linear analyses were developed accounting for both material and geometrical nonlinearities as well as for the enhanced material strain-hardening properties due to cyclic loading. In the following, all initial conditions related to this numerical reproduction are described.

3.1 Geometry

The geometry of the I-shaped links was based on the geometrical nominal values and proportions defined by a standard profile IPE550 with additional transverse stiffening as shown in Figure 2. Parametric variations of this geometry were performed systematically (see section 4). These elements were numerically reproduced using shell elements for the web, flanges and additional stiffeners. The elements were provided with plates at both ends as well as intermediate transverse stiffeners. The shell geometry was elaborated with the S4R four-noded element provided in Abaqus libraries. After a convergence analysis available in [62], a mesh size of 25 mm in all quadrilateral elements was chosen.

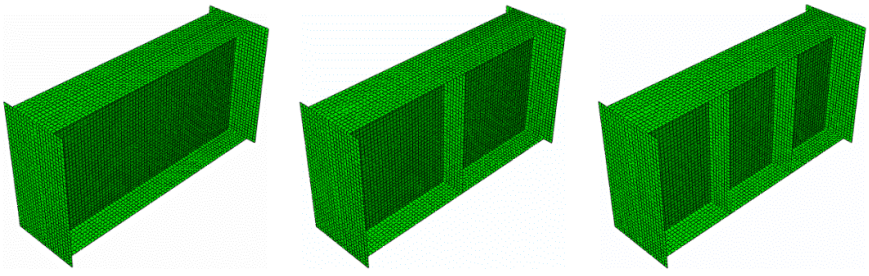

Figure 2. Different geometrical configuration of the I-shaped links.
a) unstiffened b) 1 intermediate stiffener c) 2 intermediate stiffeners

3.2 Material

The simulated links were provided with standard stainless steel (Grade 1.4301) as well as standard S355 carbon steel for the sake of comparison. For the former, a nonlinear σ-ε relationship is included whereas for the latter, an elastic-plastic relationship with strain hardening is assumed. On the other hand, the cyclic properties of the stainless steel are collected from previous research found in the literature [38] and implemented in Abaqus Simulia in the form of a combined isotropic/kinematic with cyclic hardening model. It has been experimentally observed that an adequate reproduction of strain-hardening in stainless steel is highly dependent on the loading history as well as on the attained strain levels. In this research, cyclic plasticity is introduced in the numerical model under the assumption of no prior knowledge of the loading history. The set of parameters that are introduced in the combined model correspond to average values reported in [38]. The material is assumed unstrained and non-stabilized at the beginning of the simulations. The set of parameters that are provided are related to the change in size of the yield surface (isotropic component, b_{iso} and $Q\infty$) as well as to the change in slope of the initial kinematic hardening modulus (kinematic component, C_{kin} and γ). On the other hand, the carbon steel hardening model is assumed as kinematic. Figure 3 displays the σ-ε uniaxial constitutive laws included in these simulations (monotonic).

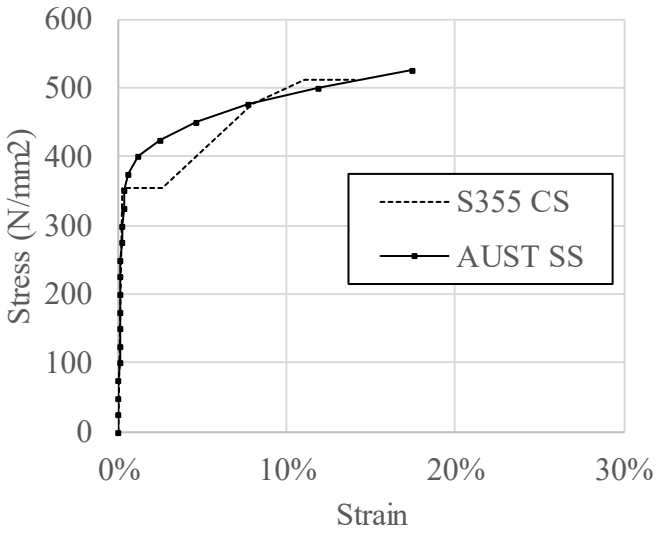

Figure 3. σ-ε uniaxial constitutive laws

3.3 Initial boundary conditions.

Isolated links were modelled with boundary conditions as suggested in [64]. The left end of the link was free to move horizontally. The right end of the link was free to move vertically. At both ends the rotation of the cross-section was not allowed. The resulting movement mimics conservatively the one obtained in elastic models of links as part of EBF systems. This boundary condition is shown in Figure 4. These conditions were evaluated in numerical simulations of full-scale models in which the links were idealized with shell elements and other non-dissipative zones were idealized using beam elements [62].

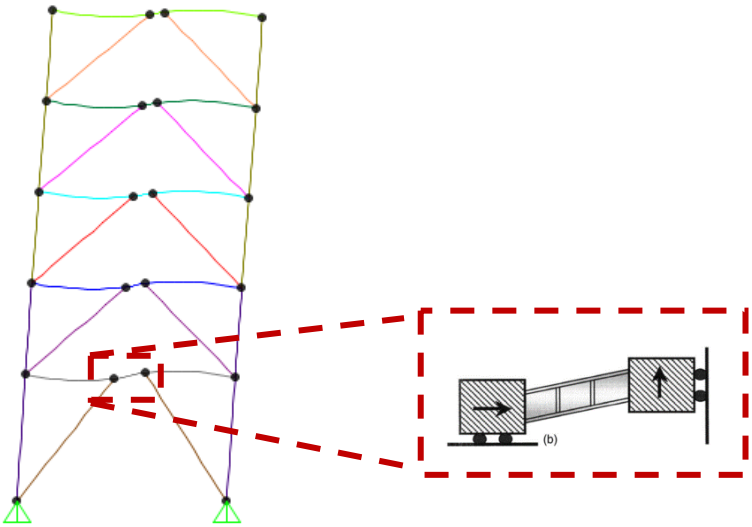

Figure 4. Initial boundary conditions for isolated members

3.4 Imperfections and residual stresses

The initial geometric imperfections as well as initial structural imperfections (residual stresses) were taking into account as is indicated in [55]. A perfectly straight geometry is perturbed by using Eigenshapes that are amplified according to the value "w" given in [55]. Residual stresses were implemented in the models with residual stress patterns suggested in [65]. The study encompasses hot-rolled and welded sections. In order to maintain comparable results, both patterns were assumed as being identical. Figure 5 displays the adopted Eigenshape as well as the residual stress pattern (values are detailed in Table 2).

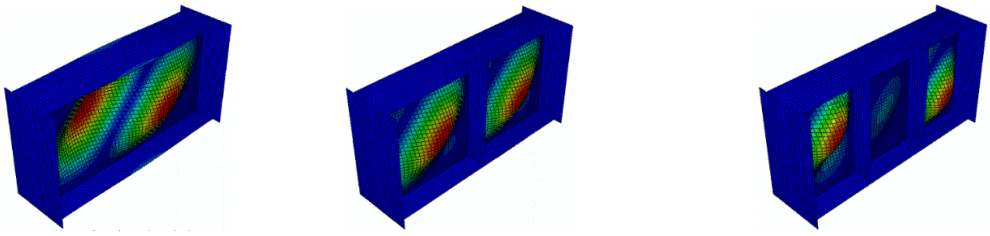

1 stiffener. 2 stiffeners 3 stiffeners

$$w=0.8\cdot\min(h_w/100;\ t_w)$$

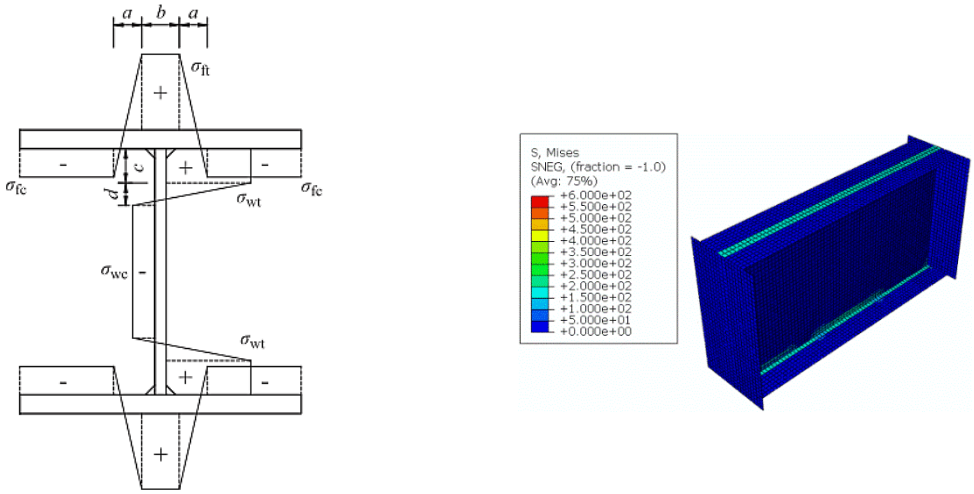

Figure 5. Initial imperfections and residual stress pattern

Material	a (mm)	b (mm)	c (mm)	d (mm)	$\sigma_{ft} = \sigma_{wt}$ (N/mm^2)	σ_{fc} (N/mm^2)	σ_{wc} (N/mm^2)
AUST 1.4301	21.0	15.8	12.9	25.8	175.0	37.12	18.10
CS S355	21.0	15.8	12.9	25.8	106.5	22.59	11.02

Table 2. Adopted values for the residual stress pattern.

3.5 Types of analysis

Three types of analysis were performed on each specimen:

i) Eigenvalue analysis from which Eigenshapes were obtained and used subsequently. This step is especially needed as an operational step for the definition of initial imperfections as depicted in Figure 5.

ii) Static GMNIA analysis, from which the shear response of the elements was analyzed. This step is especially needed as an operational step for the definition of levels of deformation and structural states (elastic, buckling, yielding). The shear static response obtained in this analysis provides information about the levels of displacement at which the web plate buckles, develops a Tension Field Action (TFA) and subsequently the system fails. An arc-length based incremental method coupled with Newton-Raphson iterative procedure are employed for the application of the monotonically increasing loading. Figure 6 displays an incremental monotonic load-displacement response.

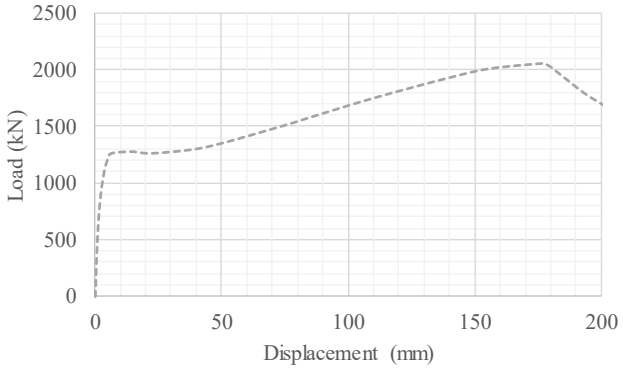

Figure 6. Static analysis (GMNIA) with increasing monotonic loading

iii) Cyclic nonlinear static analysis accounting for geometrical and material nonlinearities from which different results related to the cyclic response of links were obtained and assessed. In these analyses, the maximum amplitude of the cyclic displacement at which the elements are subjected is a key variable. For all levels of displacement, the analysis included ten accomplished cycles during sixty seconds following a sinusoidal shape. Depending on the magnitude of the displacement, the web of the link may have buckled and/or yielded during the cyclic episode. All comparisons are performed under the assumption that no fracture is attained in the material during these cycles. A dynamic implicit analysis with moderate dissipation has been used. Figure 7 displays the adopted cyclic loading protocol.

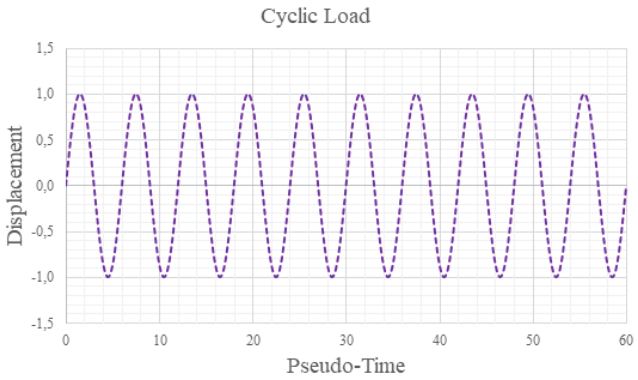

Figure 7. Loading protocol for the cyclic nonlinear static analysis

3.6 Validation

A reproduction of one of the experimental tests provided in [16] was used for validation purposes. The chosen specimen corresponds to a short link (ρ=1,04) to which the loading protocol defined in [29] was applied (version to date). The reported tests are based on an experimental program on ASTM A992 carbon steel. The protocol included a set of elastic cycles that were sequentially increased every two cycles. Increments of 0,01 rad were applied systematically until failure. In [16], the chosen tests is referred toas 4A. The shear-rotation cyclic plot is included in [16] and reproduced in Figure 8. The reproduction does not include the failure mode since fracture in the stiffener weld was reported and the model is not able to reproduce such brittle failure mode.

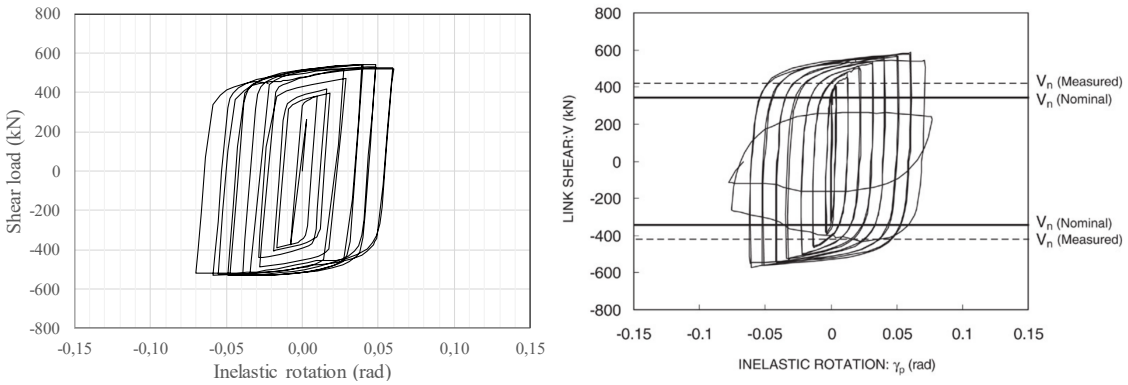

Figure 8. Numerical reproduction of 4A test presented in [16].

4. Parametric study

The numerical study consists of a set of 324 analysis on links subjected to cyclic loading. The parameter variation was conceived for the sake of assessing material, geometry, presence of axial force and level of cyclic displacement. Basically, the I-section was idealized with a standard IPE550. However, certain geometric variations (such as modification of web thickness) were also included for the sake of assessing the web slenderness. This modification results in geometries that slightly differ from the standard profile (and that would require a welded section). Figure 9 shows the set of parameters that were varied in the study. The following remarks are worth pointing out:

- Both carbon and stainless steel links were studied.

- Three different values for web thickness were studied. IPE550 has a standard value of t_w=11,1mm. Two additional values of t_w were included in order to assess the web buckling susceptibility using the same overall geometry.

- Three transverse stiffeners configurations were studied as shown in Figure 2.

- Three levels of axial load were included in the link. The axial force was quantified as a proportion of the link squash load. The values range from 0% to 15%, which is the limit that changes the shear-axial force interaction in most guidelines. According to [22-23], the presence of an axial force on the link up to a level of 15% of its squash load does not require the verification of interaction.

- Six levels of cyclic deformation were studied. These values range from 0,3% to approximately 30% principal strain levels in the web panels (corresponding to defined values of lateral displacement). The chosen zones (A-F) cover the structural cases depicted in 2.1 (elastic, buckling, post-buckling, yielding). For relatively low levels of cyclic strain (0,3% to 2,9%), the number of cycles to which the links are subjected (10) are expected to be accomplished without any problem associated with fracture mechanics. For other cases, the number of cycles is considerably high when compared to the reported adjustments of Coffin-Manson expressions on cold-worked and hot-rolled stainless steel coupons [38]. Since the numerical model does not reproduce any failure related to fracture, all cases are assumed to accomplish that number of cycles.

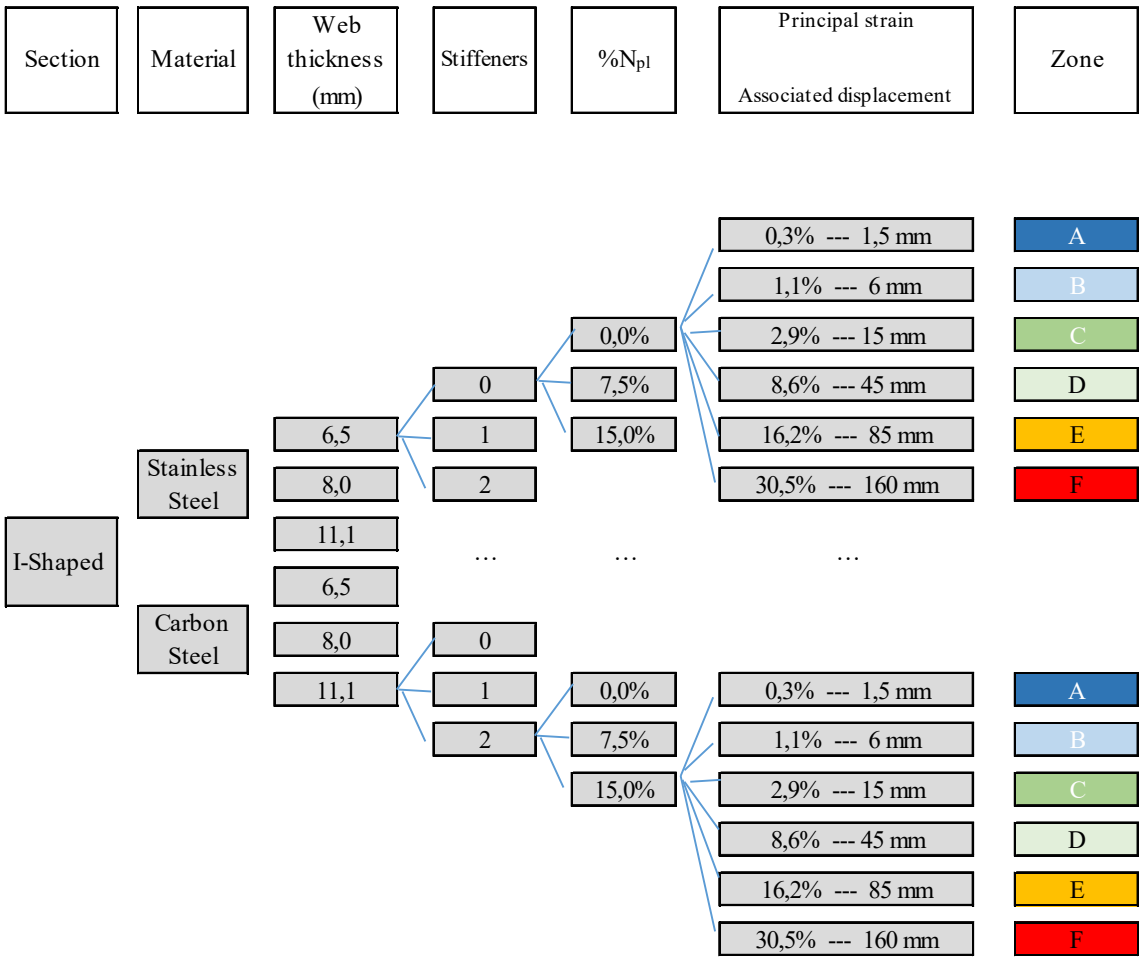

Figure 9. Variation of the numerical study

5. Results

5.1 Buckle analysis

Elastic buckle analyses were performed for the sake of inferring adequate initial imperfections that are subsequently included in GMNIA analyses. Figure 10 shows isometric views of the first Eigenvalues and Eigenshapes for 9 cases, varying t_w as well as the number of stiffeners. In all cases, Eigenshapes show shear-buckling related modes. Increasing the web thickness t_w provides an increment in critical buckling loads accordingly. These analyses were performed in a structural system in which displacements at the link ends were applied according to Figure 4. Reaction forces obtained in stress-strain analysis with similar systems were also performed for the sake of relating displacement and critical buckling loads.

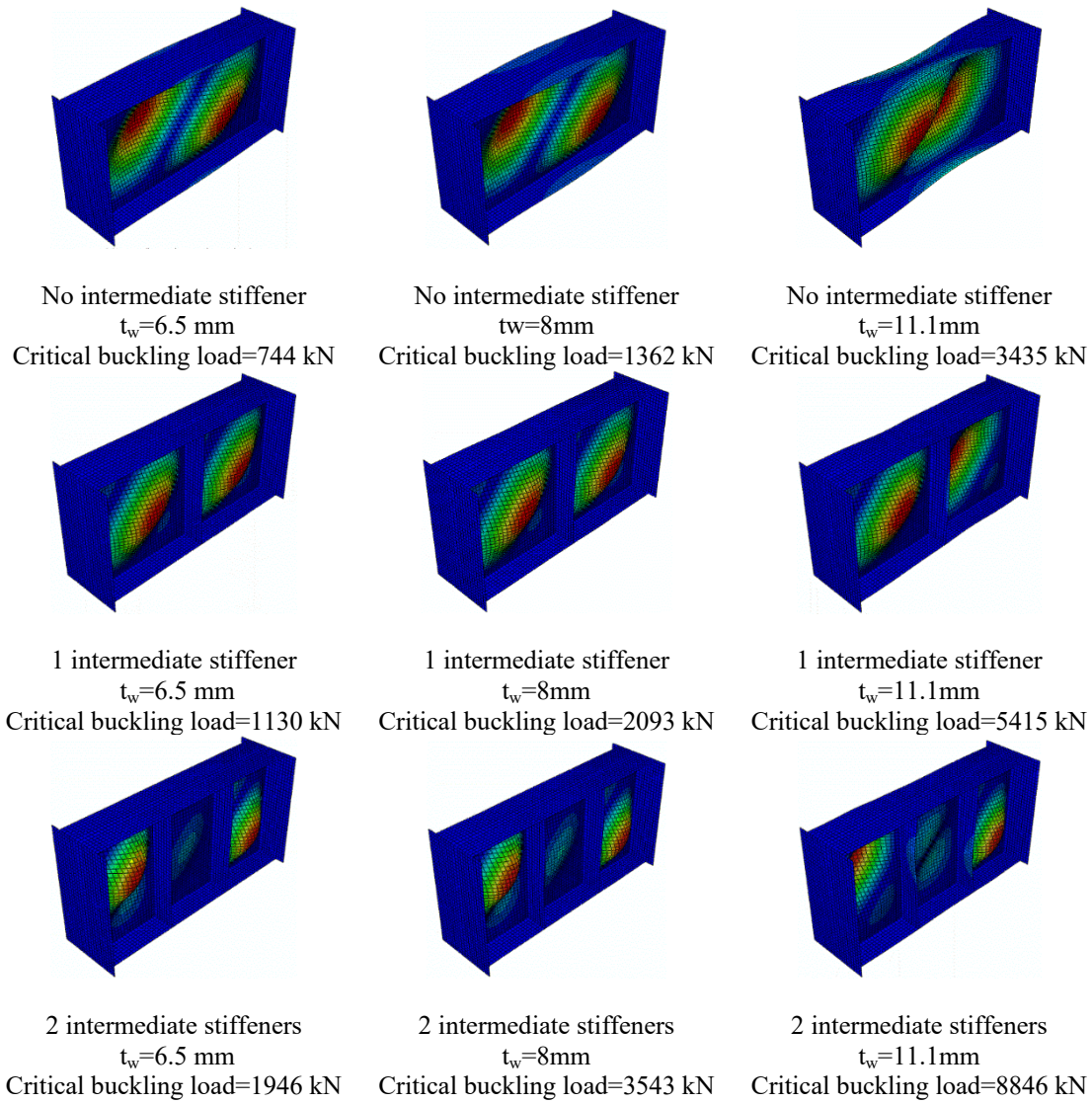

Figure 10. Eigenvalues and Eigenshapes for links with varying t_w and number of stiffeners

5.2 Static analysis

The response of the links subjected to monotonic increasing loading was obtained by means of GMNIA analyses. Results for these cases are presented separately in Figures 11 to 13 for a sample of the parametric study. In all cases, both stainless steel and carbon steel S355 are displayed. In addition, all plots include vertical lines at different values of displacement that depict the previously defined zones A to F. Figure 11 shows the static shear response of both austenitic (a) and carbon (b) steel links with varying values of web thickness. Other magnitudes such as the number of stiffeners (0) and the amount of axial load (0%) are held constant in this analysis. All plots depict a structural response that is generally found in I-sections subjected to shear buckling with a loss of linearity due to buckling, a post-buckling reserve and failure at ultimate load. For all cases, the members assembled with austenitic stainless steel provide higher ductility and ultimate load capacity. Expectedly, both buckling- as well as ultimate loads increase with the web thickness. Comparing both series of results, one observes that for a given value of displacement (e.g., those depicting the zones), the structural response lies differently in stainless steel sections when compared to the carbon steel ones.

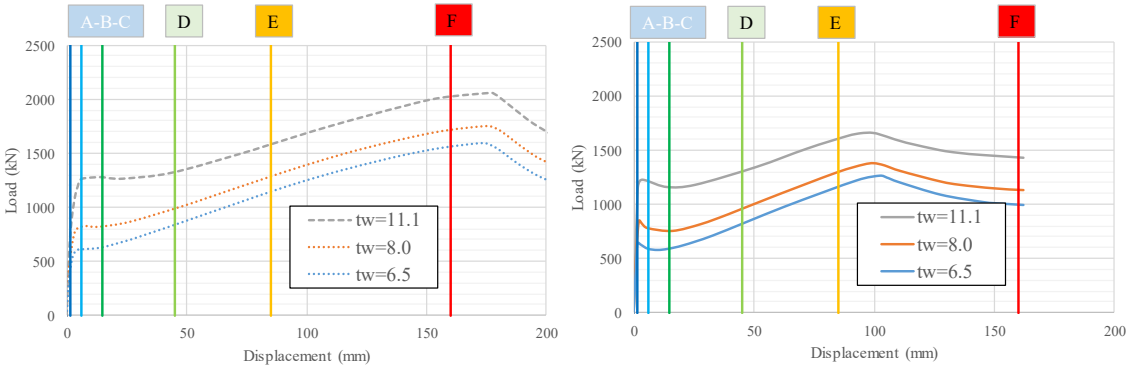

Figure 11. Static response. Variation of web thickness (a) Austenitic SS (b) S355 CS

Another series of plots are presented for the case in which the webs are transversally stiffened with 1 or 2 vertical elements in Figure 12 (the unstiffened element is also included). In this case, other magnitudes such as the web thickness (6,5mm) and the amount of axial load (0%) were held constant. More ductility and higher strength are noticeable in the stainless steel elements. The variation in the number of stiffeners improve ultimate load and ductility only slightly.

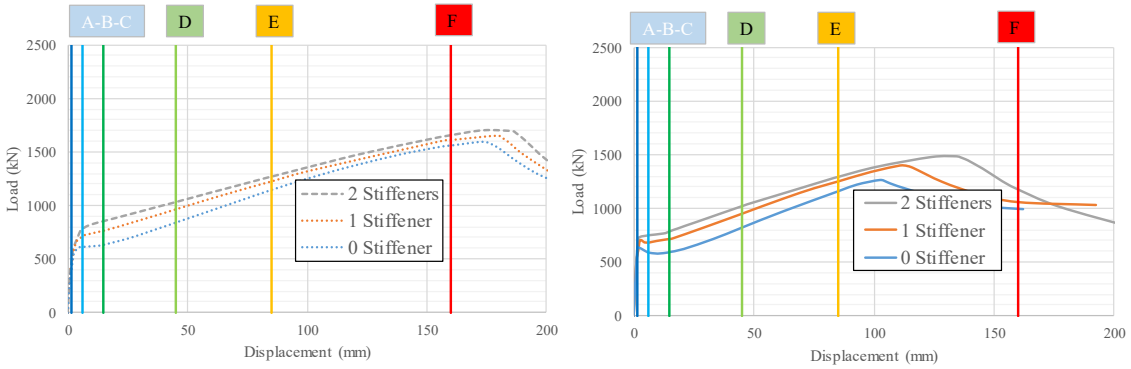

Figure 12. Static response. Transverse stiffening. (a) Austenitic SS (b) S355 CS

Finally, in Figure 13, plots are presented for the case in which varying values of axial load are included during the application of incremental shear loading. Similarly, other magnitudes such as the web thickness (6,5mm) and the number of stiffeners (0) are held constant. For both

austenitic and carbon steel, the presence of axial load plays a negligible role in their structural responses. Again, more ductility and higher strength are observed in the stainless steel elements.

For all cases (including the cases not included in the sample), common characteristics of the results are worth pointing out:

- Zones A-B-C are located near the point at which the web buckles.
- In the links simulated with austenitic steel, zones D-E-F are located in the post-buckling branch. In the links simulated with carbon steel, zones D and E are located in the post-buckling branch but F is located after the ultimate load.
- In all comparable cases, the ultimate load capacity as well as the displacement at which this load occurs are higher in stainless steel elements than in carbon steel elements. These observations are quantified in Table 3.

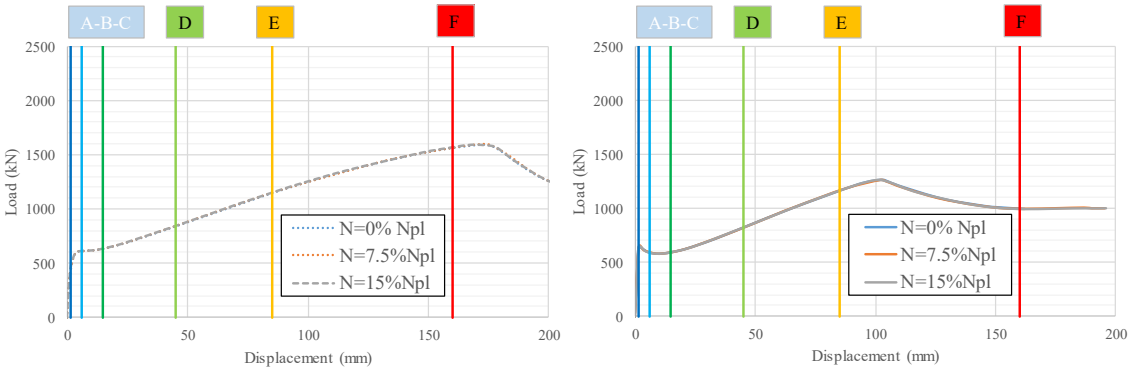

Figure 13. Static response. Axial load $\%N_{pl}$. (a) Austenitic SS (b) S355 CS

Parameter		Austenitic Stainless Steel		Carbon Steel		Comparison	
		$F_{u,ss}$ (kN)	$\delta_{u,ss}$ (mm)	$F_{u,cs}$ (kN)	$\delta_{u,cs}$ (mm)	$F_{u,ss}/F_{u,cs}$	$\delta_{u,ss}/\delta_{u,cs}$
t_w (mm)	6,5	1596,28	173,68	1258,56	102,40	1,27	1,70
	8	1745,98	175,07	1381,48	99,77	1,26	1,75
	11	2056,78	177,38	1660,15	99,64	1,24	1,78
Stiffeners	0	1596,28	173,68	1258,56	102,40	1,27	1,70
	1	1653,73	179,55	1393,82	112,35	1,19	1,60
	2	1703,96	173,58	1484,60	134,52	1,15	1,29
$\%N_{pl}$	0	1596,28	173,68	1258,56	102,40	1,27	1,70
	7,5	1596,23	170,11	1260,76	104,64	1,27	1,63
	15	1591,64	167,86	1260,35	100,31	1,26	1,67

Table 3. Variation on ultimate load capacity and ductility for the studied links. Static loading

5.3 Cyclic analysis

Cyclic nonlinear static analysis accounting for geometrical and material nonlinearities were performed for variable levels of cyclic displacement. These displacements are related to the zones defined in 5.2. From these analyses, three types of results are extracted and compared for links assembled with both stainless and carbon steel: i) shear load, ii) energy dissipation and iii) residual displacement. Generally, the analyses are compared directly between stainless steel and carbon steel links after achieving ten cycles of displacement for all zones. Results are selected from the parametric study in samples. Other cases show identical results and may be extrapolated.

- For the analysis of shear load, the plotted results are related to the cases with no intermediate stiffeners, t_w=6,5mm and N=0%N_{pl}.
- For the analysis of energy dissipation, the plotted results are related to the cases with 2 intermediate stiffeners, t_w=6,5mm and N=0%N_{pl}.
- For the analysis of residual displacement, the plotted results are related to the cases with varying t_w, varying number of stiffness and for illustration, N=7,5%N_{pl}.

One important remark, however, needs to be pointed out. Zone F in stainless steel links lies in the post-buckling range whereas in carbon steel this level of displacement is attained in the post-failure branch. In such cases, due to premature failure, cyclic loading was developed in a limited number of cycles. Consequently, these zones are not compared directly one another since they neither correspond to the same structural initial condition nor number of cycles. Furthermore, it is highlighted that in some cases of CS links, the analysis was not completed for ten cycles due to lack of convergence. These results are not compared either.

5.3.1 Shear load

The shear load is defined as one of the magnitudes of comparison in this study. Statically, all zones define levels of displacement with an associated shear load that is read directly from the response curve. Cyclically, if this level of displacement is applied during ten cycles, the system may either harden or soften as a function of the geometry, material and initial displacement. Figures 14 and 15 display the cyclic response for both austenitic and carbon steel links separately for zones A-B-C (elastic, pre-buckling and buckling) and D-E-F (post-buckling, yielding and hardening) respectively. The following observations can be pointed out:

- In Figure 14, for zone A, the cyclic displacement in SS links is slightly nonlinear due to material effects. In CS links for this level of displacement, the material remains elastic. For zones B and C, SS links show rounded cyclic responses whereas CS links show a more pronounced yield point. The values of shear are similar in both cases. These zones correspond to areas at which shear buckling occurs for both SS and CS links. A coupled nonlinear mechanical phenomenon of plate buckling and post-buckling Tension Field Action (TFA) mechanism begins to be observable. In SS links, material strain-hardening is also coupled with this geometric and mechanical behavior due to inelastic buckling. Since the level of deformation in zones A-B-C is relatively low, none of both materials have achieved full strain hardening at this level.

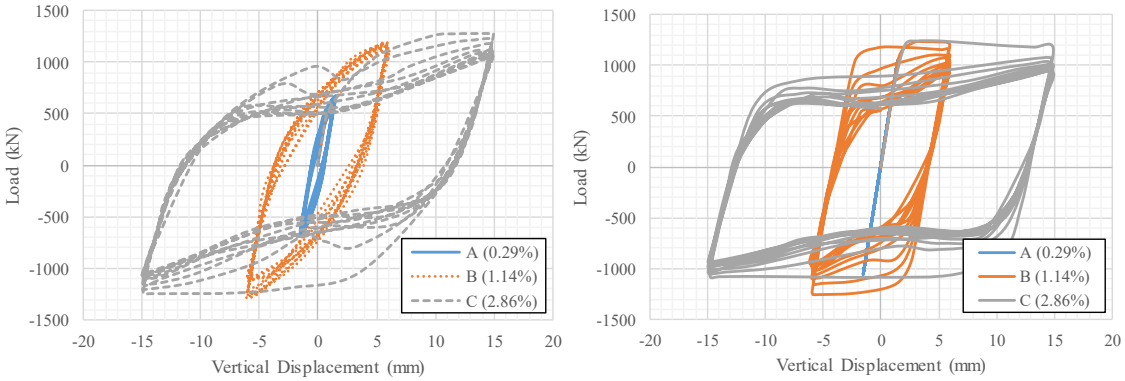

Figure 14. Response for cyclic displacement in zones A-B-C.
(a) Austenitic SS (b) S355 CS

- In Figure 15 strain-hardening in SS links for consecutive cycles of loading is noticeable. In CS links though, no increment in shear load for consecutive cycles is observed. SS links are more deformable and resistant than their CS counterparts (under the assumption of no failure for this amount of cycles). In zone D, SS links exhibit

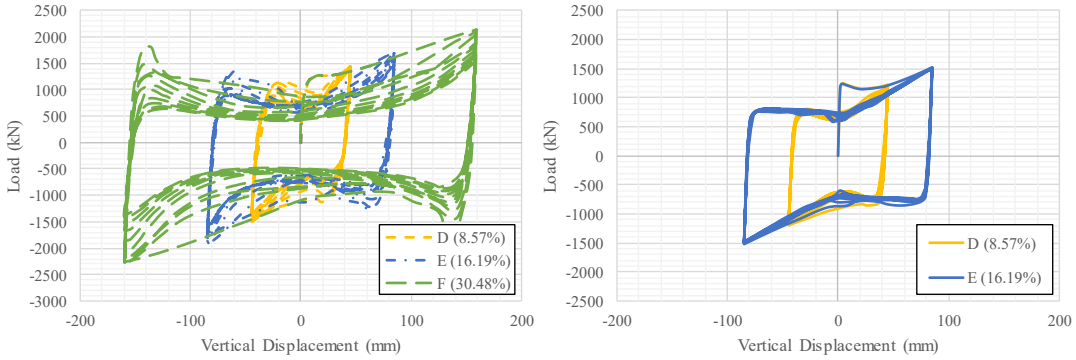

- Figure 15. Response for cyclic displacement in zones D-E-F.
- (a) Austenitic SS (b) S355 CS

Table 4 shows the results obtained in stainless steel links under both static and cyclic loading. The results are organized in such a way that the influence of web thickness and the transverse stiffening are displayed. Table 5 shows a similar organization of results but in this case, obtained with carbon steel links.

Several conclusions are worth pointing out:

- In SS links, for low level of displacement (zones A-B-C, results bolted in Table 4), shear load after cyclic loading increase only marginally. In some cases, the obtained value of cyclic shear load decreases slightly. However, for high values of displacement (zones D-E-F), the increment in shear load is noticeable for all values of t_w and number of stiffeners. Strain hardening plays a greater role for the case in which the resistant mechanism of the links involves TFA in the web with the progressive development of the frame mechanism in the flanges. These results suggest emphasis must be put on the material modelling. Since the cyclic plasticity parameters were kept constant in this study, additional research may be necessary in which hardening of the material is systematically varied. Experimental results presented in SS coupons subjected to extremely low fatigue show that strain-hardening depends on the cyclic loading history as well.

Web thickness (mm)	Zones	δ_{ss} (mm)	0 Stiffeners		1 Stiffener		2 Stifferners	
			Static	Cyclic	Static	Cyclic	Static	Cyclic
			$F_{ss,static}$ (kN)	$F_{ss,10\ cycles}$ (kN)	$F_{ss,static}$ (kN)	$F_{ss,10\ cycles}$ (kN)	$F_{ss,static}$ (kN)	$F_{ss,10\ cycles}$ (kN)
t_w=6,5	**A**	**1,5**	**387,44**	**398,16**	**410,99**	**426,09**	**458,95**	**423,91**
	B	**6**	**612,99**	**563,12**	**708,33**	**697,62**	**778,83**	**787,03**
	C	**15**	**634,29**	**618,86**	**766,73**	**783,10**	**856,07**	**904,95**
	D	45	840,37	899,27	965,37	1054,30	1033,23	1223,48
	E	85	1144,84	1258,15	1226,88	1376,38	1271,38	1477,87
	F	160	1561,10	1766,51	1613,95	1786,16	1659,04	1812,87
t_w=8	**A**	**1,5**	**502,79**	**484,07**	**545,35**	**496,96**	**555,59**	**497,44**
	B	**6**	**809,37**	**762,17**	**915,25**	**951,09**	**942,33**	**1058,54**
	C	**15**	**822,77**	**806,21**	**972,54**	**985,76**	**1050,45**	**1180,33**
	D	45	985,85	1074,25	1132,49	1291,98	1212,10	1494,77
	E	85	1281,22	1471,23	1383,03	1618,52	1442,83	1735,97
	F	160	1706,13	1937,51	1773,89	2009,93	1813,17	2045,81
t_w=11,1	**A**	**1,5**	**679,80**	**673,41**	**735,68**	**683,76**	**740,53**	**685,89**
	B	**6**	**1249,56**	**1291,84**	**1260,57**	**1414,50**	**1265,41**	**1499,38**
	C	**15**	**1280,64**	**1274,47**	**1393,41**	**1505,17**	**1452,47**	**1924,64**
	D	45	1325,90	1508,66	1518,35	1748,28	1648,62	2030,16
	E	85	1580,09	1920,81	1713,07	2052,84	1828,95	2258,71
	F	160	2019,71	2284,07	2110,59	2293,36	2163,97	2491,53

Table 4. Shear load attained for static and cyclic loading for different displacement zones. Austenitic stainless steel

- In CS links, for low level of displacement (zones A-B-C, results bolted in Table 5), shear load after cyclic loading increase in most cases. However, for high values of displacement (zones D-E-F), the results are not satisfactory (the number of cycles was not achieved, the material hardening does not contribute or simply, the results are not comparable. Additional research may also be necessary in which strain-hardening in carbon steel is systematically varied as well.

Web thickness (mm)	Zones	δ_{cs} (mm)	0 Stiffeners		1 Stiffener		2 Stifferners	
			Static	Cyclic	Static	Cyclic	Static	Cyclic
			$F_{cs,static}$ (kN)	$F_{cs,10\ cycles}$ (kN)	$F_{cs,static}$ (kN)	$F_{cs,10\ cycles}$ (kN)	$F_{cs,static}$ (kN)	$F_{cs,10\ cycles}$ (kN)
t_w=6,5	A	1,5	**612,37**	**679,53**	**557,79**	**681,65**	**564,61**	**684,92**
	B	6	**589,02**	**623,54**	**681,15**	**703,51**	**750,59**	**763,89**
	C	15	**592,37**	**634,37**	**713,83**	**712,42**	**787,37**	**782,51**
	D	45	817,49	781,94	947,23	900,44	1020,60	not achieved
	E	85	1153,28	not achieved	1245,81	not achieved	1293,14	not achieved
	F	160	---	---	---	---	---	---
t_w=8	A	1,5	**617,59**	**806,61**	**805,35**	**814,26**	**775,59**	**806,91**
	B	6	**782,66**	**843,72**	**865,25**	**892,99**	**912,33**	**940,69**
	C	15	**761,01**	**838,69**	**897,54**	**894,87**	**960,45**	**983,02**
	D	45	960,36	910,76	1122,49	1053,23	1212,10	not achieved
	E	85	1299,46	not achieved	1413,03	not achieved	1472,83	not achieved
	F	160	---	---	---	---	---	---
t_w=11,1	A	1,5	**989,31**	**1062,77**	**1023,52**	**1061,08**	**1084,44**	**1066,90**
	B	6	**1216,08**	**1253,00**	**1258,36**	**1283,30**	**1266,25**	**1291,54**
	C	15	**1162,94**	**1239,49**	**1270,84**	**1307,43**	**1323,22**	**1364,71**
	D	45	1307,69	not achieved	1499,81	not achieved	1619,72	not achieved
	E	85	1605,40	not achieved	1769,12	not achieved	1877,60	not achieved
	F	160	---	---	---	---	---	---

Table 5. Shear load attained for static and cyclic loading for different displacement zones. Carbon steel

5.3.2 Energy dissipation

Results related to energy dissipation due to plastic deformation are also provided by the implemented numerical model. These results are associated to work only and not to potential heat dissipation during the plastic deformation process. Figures 16 and 17 show the evolution of plastic energy dissipation (in Joules) throughout time for all A-B-C and D-E-F zones respectively. Closer inspection on such plots allows pointing out several remarks:

- For low values of displacement, Figure 16 energy dissipation in both SS and CS links is low with similar values. In zone A, SS links begin energy dissipation due to the material nonlinearity at low strain levels. The CS counterparts in zone A (pre-yielding in CS) do not dissipate energy (it is only stored).

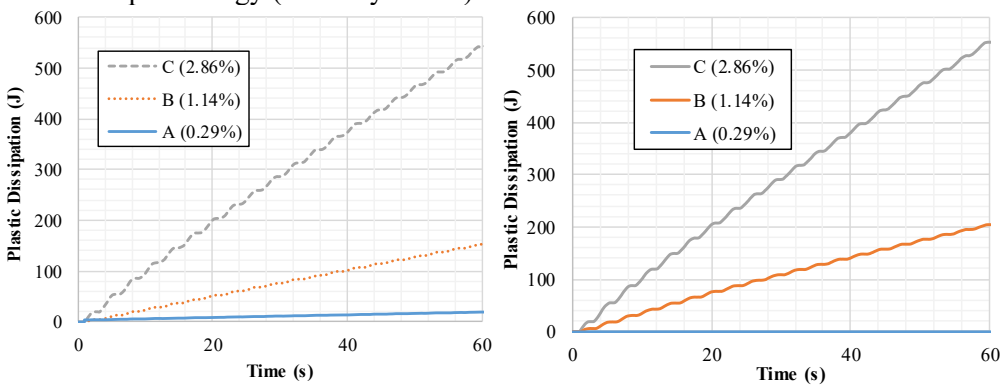

Figure 16. Accumulated energy dissipation during cyclic loading for low displacement (A-C) (a) Austenitic SS (b) S355 CS

- For high values of displacement, Figure 17 shows that energy dissipation in SS is considerably greater than in the CS counterparts. Zone F is only displayed for SS links. Noticeably, the energy accumulation in 10 cycles increases with the initial level of deformation quite considerably. The accumulated energy for the CS links is presented up to the point at which the analysis stopped due to convergence.

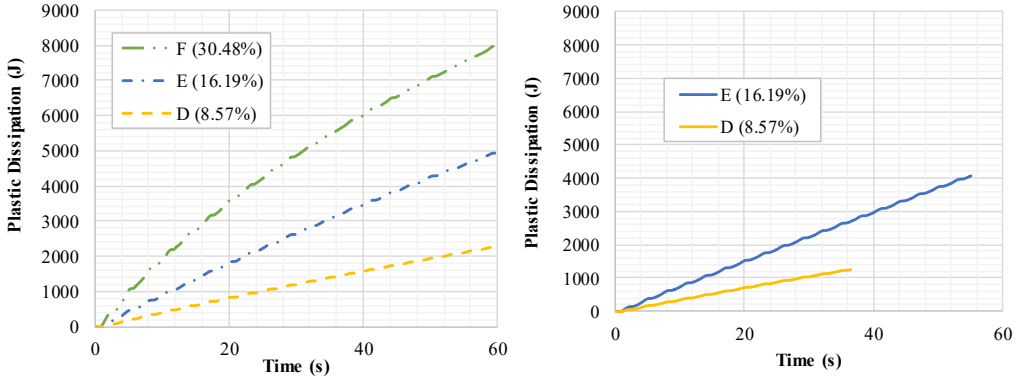

Figure 17. Accumulated energy dissipation during cyclic loading for high displacement (D-F) (a) Austenitic SS (b) S355 CS

Table 6 shows all results obtained for different web thicknesses and transverse stiffening. For all cases, the level of axial force equals $N=0\%N_{pl}$. Only results accomplishing ten cycles of loading are reported (other cases are indicated as not achieved or alternatively, not comparable). Energy dissipation is generally greater in SS links. In zone A, due to material nonlinearity at low strain levels, SS links begins energy dissipation considerably. For zones B and C (buckling, post-buckling), energy dissipation is slightly higher for CS links. For high levels of plastic strain (D-E-F), SS links achieve proper convergence with a considerable energy dissipation level. CS do not provide comparable results (low convergence).

Web thickness (mm)	Zones	$\delta_{10\ cycles}$ (mm)	Energy dissipation (J)					
			Austenitic stainless steel			Carbon steel		
			Stiff=0	Stiff=1	Stiff=2	Stiff=0	Stiff=1	Stiff=2
t_w=6,5	A	1,5	12,6	32,9	17,6	1,3	0,8	0,2
	B	6,0	80,6	111,5	153,7	96,3	145,9	205,5
	C	15,0	281,4	382,9	548,5	317,4	465,0	562,5
	D	45,0	1.277,5	1.706,6	2.294,4	1.308,1	1.680,9	not achieved
	E	85,0	3.091,7	3.789,0	5.013,7	not achieved	not achieved	not achieved
	F	160,0	6.464,8	7.372,4	8.102,2	---	---	---
t_w=8	A	1,5	16,0	16,3	16,6	1,1	0,3	0,0
	B	6,0	117,0	164,7	204,4	138,0	198,2	283,5
	C	15,0	385,9	538,0	765,0	453,9	619,6	757,6
	D	45,0	1.734,2	2.275,0	2.971,7	1.580,0	2.202,0	not achieved
	E	85,0	3.780,6	4.838,0	6.148,4	not achieved	not achieved	not achieved
	F	160,0	8.243,2	8.359,2	9.170,8	---	---	---
t_w=11,1	A	1,5	30,1	21,4	23,3	0,1	0,0	0,0
	B	6,0	239,9	267,5	279,6	265,5	374,6	403,0
	C	15,0	653,2	968,6	1.316,1	770,6	996,2	1.244,5
	D	45,0	2.908,6	3.641,0	4.561,6	not achieved	not achieved	not achieved
	E	85,0	5.824,0	7.328,3	7.922,6	not achieved	not achieved	not achieved
	F	160,0	11.046,3	8.807,7	9.621,7	---	---	---

Table 6. Energy dissipation accumulated at 10 cycles for all zones, web thickness and transverse stiffening.

5.3.3 Residual displacement

The residual displacement value in the links for both material types, web thicknesses and intermediate stiffeners quantity are shown in Table 7. The residual displacement is larger for SS links. When intermediate stiffeners are used, the residual displacement value decreases, which may be an interesting alternative for the case in which links are meant to be replaced after energy dissipation episodes. It is observed that increasing the number of stiffeners may enhance this feature as well as other comparison magnitudes. Figure 18 shows a series of isometric views of SS links after achieving ten cycles for different zones and stiffening configurations. Expectedly, the presence of transverse stiffeners divide panels in a beneficial fashion.

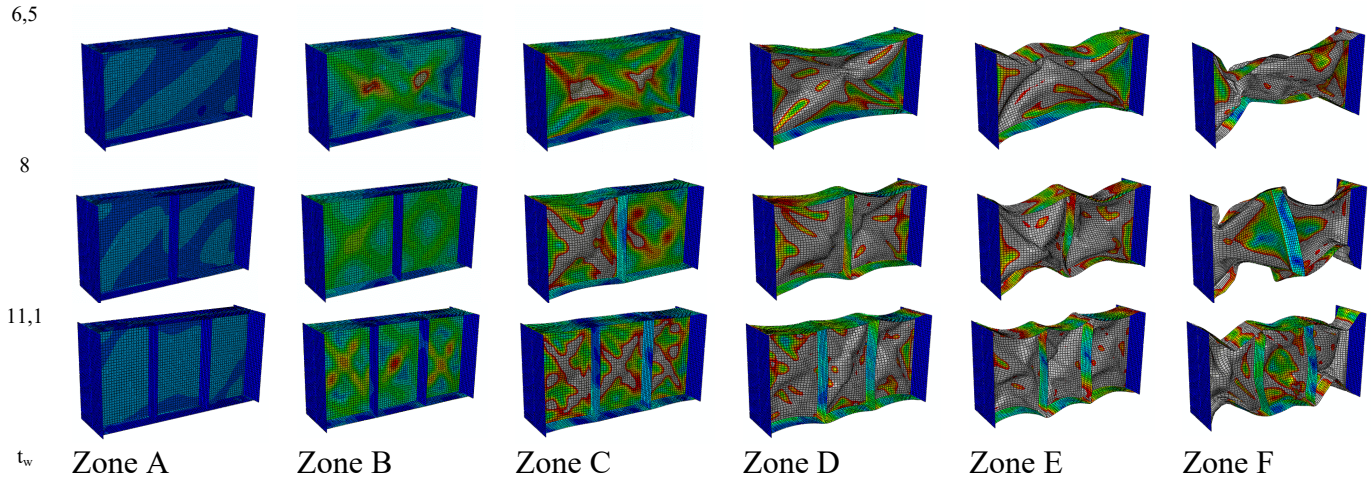

Figure 18. Residual displacement in links after 10 cycles in austenitic SS links for all zones with varying web stiffening

Table 7 displays absolute values of vertical residual displacement at mid-span of the links. For the case in which no additional stiffeners are included, this displacement is clearly higher. For low levels of cyclic displacement (A-B-C zones) SS links show a marginally higher value due to the initial development of material nonlinearity. For the cases of high values of cyclic displacement, results are not fully compared since some of the CS links did not accomplish such cyclic loading.

Web thickness (mm)	Zones	$\delta_{10\ cycles}$ (mm)	Residual displacement at mid-span (mm)					
			Austenitic stainless steel			Carbon steel		
			Stiff=0	Stiff=1	Stiff=2	Stiff=0	Stiff=1	Stiff=2
t_w=6,5	A	1,5	0,24	0,01	0,23	0,02	0,00	0,00
	B	6,0	5,71	0,05	0,28	5,57	0,77	0,83
	C	15,0	21,08	0,42	2,56	11,53	3,72	2,28
	D	45,0	61,74	9,82	22,41	43,56	21,05	not achieved
	E	85,0	61,97	23,14	61,51	not achieved	40,40	not achieved
	F	160,0	221,25	36,02	55,45	---	---	---
t_w=8	A	1,5	0,07	0,01	0,06	0,00	0,00	0,00
	B	6,0	5,10	0,14	0,17	5,16	0,83	0,57
	C	15,0	22,55	0,27	1,36	7,85	4,26	0,03
	D	45,0	71,28	7,76	1,37	44,12	21,83	not achieved
	E	85,0	72,11	22,05	6,36	not achieved	not achieved	not achieved
	F	160,0	200,26	12,39	18,98	---	---	---
t_w=11,1	A	1,5	0,02	0,01	0,01	0,00	0,00	0,03
	B	6,0	2,71	0,09	0,01	4,20	0,79	403,04
	C	15,0	21,02	2,39	1,11	6,47	0,13	1.244,50
	D	45,0	66,50	25,77	2,11	not achieved	not achieved	not achieved
	E	85,0	109,25	49,10	10,49	not achieved	not achieved	not achieved
	F	160,0	180,80	5,03	15,08	---	---	---

Table 7. Residual displacement after 10 cycles for all zones, with varying web thickness and transverse stiffening.

6. Conclusions and future remarks

In this paper, a numerical study on links on eccentrically braced frames is developed and presented. Numerical models focused on isolated links on stainless and carbon steel subjected to both monotonic and cyclic loading were developed. Several geometrical and loading configurations were studied with particular observations regarding their effects on the cyclic response. The study is focused in cyclic loading with constant amplitude for the sake of evaluating the differences at pre-buckling, buckling and yielding stages.

Shear load, energy dissipation and residual displacement were used as comparative features.

- Stainless steel links provide an interesting solution as structural fuses in eccentrically braced frames. At low levels of cyclic displacement, their behavior is similar to the one observed in their carbon steel counterparts. However, for severe levels of cyclic displacement, strain-hardening and energy dissipation in SS links outperform identical CS elements.

- The presence of transverse stiffening enhance the overall behavior of the links as expected. A particular beneficial aspect may be related to the residual displacement control. In particular, replaceable SS links (that may be an interesting alternative structural fuse) require these types of control after severe loading episodes.

- The effect of axial loading has been found negligible in the studied range. Both European and American codes define a limit ($N=15\%N_{pl}$) under which this effect may be neglected. The results obtained confirm the validity of such limitations in SS links.

Finally, it is worth pointing out that the study was developed under the assumption of no fracture of the material during cyclic loading. The potential effect of the material modelling assumptions (variable cyclic plasticity for different strain levels) needs to be investigated to a greater extent in both cases (SS and CS links).

Acknowledgements

This work was developed in the frame of the Project BIA2016-75678-R, AEI/FEDER, UE "Comportamiento estructural de pórticos de acero inoxidable. Seguridad frente a acciones accidentales de sismo y fuego", funded from the MINECO (Spain).

References

[1] Fujimoto M., Aoyagi T., Wada A., Saito K. Structural characteristics of eccentric K-braced frames. Trans. Arch. Inst. Jpn. 195, 39-49 (1972). *In japanese*

[2] Tanabashi R., Naneta K., Ishida T., On the rigidity and ductility of steel bracing assemblage, Proceedings of the 5th World Conference on Earthquake Engineering, IAEE, Rome 834-840 (1974).

[3] Hjelmstad K., Popov E. Cyclic behavior and design of links beams. Journal of Structural Engineering ASCE, 109 (10), 2387-2403. (1983)

[4] Kasai K., Popov E. General behavior of WF steel shear link beams. Journal of Structural Engineering ASCE, 112 (2), 362-382. (1986).

[5] Engelhardt M., Popov E. Experimental performance of long links in eccentrically braced frames. Journal of Structural Engineering ASCE. 118(11), 3067-3088. (1992)

[6] Roeder C., Popov E. Eccentrically braced steel frames for earthquakes. Journal of Structural Division. ASCE. 104(3), 391-412. (1978)

[7] Engelhardt M., Popov E. On design of eccentrically braced frames. Earthquake Spectra. 5 (3), 495-511. (1989)

[8] Popov E., Engelhardt M., Ricles J. Eccentrically braced frames: U.S. practice. Engineering Journal. 26. 2nd Quarter, 66-80. (1989)

[9] Baddoo N., Stainless steel in construction: A review of research, applications, challenges and opportunities. Journal of Constructional Steel Research, 64 (11), 1199–1206, (2008)

[10] Bosco M., Marino E., Rossi P.P. Influence of modelling of steel link beams on the seismic response of EBFs, Engineering Structures 127, 459-474, (2016)

[11] Bosco M, Marino EM, Rossi PP. Modelling of steel link beams of short, intermediate or long length. Engineering Structures, 84, 406–18.(2015)

[12] Ramadan T, Ghobarah A. Analytical model for shear-link behaviour. Journal of Structural Engineering ASCE. 121(11), 1574–80. (1995)

[13] Moammer, O., Dolatshahi, K.M. Predictive equations for shear link modeling toward collapse. Engineering Structures, 151, pp. 599-612. 2017

[14] Mansour N., Christopoulos C., Tremblay R. Experimental validation of eccentrically braced frames, Journal of Structural Engineering ASCE, 137(10), 1141-1152, (2011)

[15] Richards P., Uang CM, Testing protocol for short links in eccentrically braced frames. Journal of Structural Engineering ASCE. 132(8), 1183-1191. (2006)

[16] Okazaki and M. D. Engelhardt. Cyclic loading behavior of EBF links constructed of ASTM A992 steel. J. Constr. Steel Res. Vol. 63(6), pp. 751–765, 2007

[17] Berman J., Bruneau M. Experimental and analytical investigation of tubular links for eccentrically braced frames, Engineering Structures 129 (8), 1929-1938, (2007)

[18] Wang F., Su M., Hong M., Guo Y., Li S., Cyclic behaviour of Y-shaped eccentrically braced frames fabricated with high-strength steel composite, Journal of Constructional Steel Research. 120, 176-187 (2016).

[19] Ioan A., Stratan A., Dubina D., Poljansek M., Molina F.J., Taucer F., Pegon P., Sabau G. Experimental validation of re-centring capability of eccentrically braced frames with removable links, Engineering Structures 113, 335-346, (2015)

[20] Mansour N., Christopoulos C., Tremblay R. Experimental validation of replaceable shear links for eccentrically braced frames, Journal of Structural Engineering ASCE. 137(10), 1141-1152, (2011)

[21] Liu, X.-G., Fan, J.-S., Liu, Y.-F., Yue, Q.-R., Nie, J.-G. Experimental research of replaceable Q345GJ steel shear links considering cyclic buckling and plastic overstrength. Journal of Constructional Steel Research, 134, pp. 160-179. 2017

[22] Montuori, R., Nastri, E., Piluso, V. Seismic response of EB-frames with inverted Y-scheme: TPMC versus eurocode provisions. Earthquake and Structures, 8 (5), pp. 1191-1214. 2015

[23] Nastri, E., Montuori, R., Piluso, V. Seismic design of MRF-EBF dual systems with vertical links: EC8 vs plastic design. Journal of Earthquake Engineering, 19 (3), pp. 480-504. 2015

[24] Montuori, R., Nastri, E., Piluso, V. Rigid-plastic analysis and moment-shear interaction for hierarchy criteria of inverted Y EB-Frames. Journal of Constructional Steel Research, 95, pp. 71-80. 2014

[25] Lian, M., Su, M. Seismic performance of high-strength steel fabricated eccentrically braced frame with vertical shear link. Journal of Constructional Steel Research, 137, pp. 262-285. 2017

[26] Mazzolani F., Corte G., D'Aniello M., Experimental analysis of steel dissipative bracing systems for seismic upgrading, Journal of Civil Engineering Managmenet. 15 (1), 7-19 (2009)

[27] Kanvinde A., Marshall K., Grilli D., Bomba G. Forensic analysis of link fractures in eccentrically braced frames during the February 2011 Christchurch Earthquake: Testing and simulation. Journal of Structural Engineering. 141(5),1-15 (2015)

[28] Kazemzadeh S., Topkaya C. A review of research on steel eccentrically braced frames, Journal of Constructional Steel Research 128, 53-73, (2017)

[29] ANSI/AISC 341-16. Seismic provisions for structural steel buildings. (2016)

[30] European Committee for Standardization Eurocode 3. EN 1998-1: Eurocode 8: Design of structures for earthquake resistance – Part 1: General rules, seismic actions and rules for buildings. (2004)

[31] Bosco, M., Ghersi, A., Marino, E.M., Rossi, P.P. Importance of link models in the assessment of the seismic response of multi-storey ebfs designed by ec8. Ingegneria Sismica, 33 (3), 82-93. 2016

[32] Hjelmstad K., Popov E. Seismic behavior of active beam links in eccentrically braced frames. EERC Report 83-15. University of California, Berkeley, CA, (1983)

[33] Pingle, A., Baskar, K. Non-linear behaviour of steel frame with aluminium shear-link. Journal of Structural Engineering (India), 44 (5), pp. 527-541. 2017

[34] Li R., Zhang Y., Tong LW. Numerical study of the cyclic load behavior of AISI 316L stainless steel shear links for seismic fuse device. Frontiers of Structural and Civil Engineering. Vol. 8(4), 4114-426. 2014

[35] Mirambell E. and Real E. On the calculation of deflections in structural stainless steel beams: an experimental and numerical investigation. Journal of Constructional Steel Research, 54(4), 109–133. (2000)

[36] Rasmussen K., Full-range stress–strain curves for stainless steel alloys. Journal of Constructional Steel Research, 59(1), 47–61. (2003)

[37] Arrayago, I., Real, E. and Gardner, L. Description of stress-strain curves for stainless steel alloys. Materials and Design, 87, 540–552. (2015)

[38] Nip K., Gardner L., Davies C., Elghazouli, A. Extremely low cycle fatigue tests on structural carbon steel and stainless steel. Journal of Constructional Steel Research, 66(1), 96-110. (2010)
[39] Ye D., Matsuoka S., Nagashima N., Suzuki N. The low-cycle fatigue, deformation and final fracture behaviour of an austenitic stainless steel. Material Science and Engineering A, 415(1-2) 104-117. (2006)
[40] Wang Y., Chang T., Shi Y., Yuan H., Yang L., Liao D. Experimental study on the constitutive relation of austenitic steel S31608 under monotonic and cyclic loading. Thin-Walled Structures, 83, 19-27. (2014)
[41] Zhou F., Li L. Experimental study on hysteretic behavior of structural stainless steel under cyclic loading. Journal of Constructional Steel Research, 122, 94-109. (2016)
[42] Chaboche J. A review of some plasticity and viscoplasticity constitutive theories". International Journal of Plasticity, 24(10), 1642-1693. (2008)
[43] European Committee for Standardization Eurocode 3. EN1993-1-4:2006+A1:2015. Design of steel structures. Part 1-4: General rules. Supplementary rules for stainless steels. Brussels, Belgium, (2015)
[44] Steel Construction Institute. Design Manual for Stainless Steel. Fourth Edition. (2017)
[45] SEI/ASCE 8-02. Specification for the design of cold-formed stainless steel structural members. American Society of Civil Engineers (ASCE), Reston, US, (2002)
[46] Gardner L. Stability and design of stainless steel structures- Review and Outlook. International Conference on Thin-Walled Structures. Lisbon, Portugal. (2018)
[47] Saliba N., Real E., Gardner L. Shear design recommendations for stainless steel plate girders, Engineering Structures 59, 220-228, (2014)
[48] Real E., Mirambell E., Estrada I. Shear response of stainless steel plate girders, Engineering Structures 29(7), 1626-1640, (2007)
[49] Hassanein F., Finite element investigation of shear failure of lean duplex stainless steel plate girders. Thin-Walled Structures.,49(8), 964–973, (2011).
[50] Chen X., Yuan Y., Du X., Zhao Y., Ye J., Yang L., Shear buckling behaviour of welded stainless steel plate girders with transverse stiffeners. Thin-Walled Structures, 122, 529–544, 2018
[51] Reis A., Lopes N., Real E., Vila-Real P. Stainless steel plate girders subjected to shear buckling at normal and elevated temperatures. Fire Technology. 53 (2), 815-843. (2017)
[52] Basler K., Yen B., Mueller J., Thürlimann B. Web buckling tests on welded plate girders. Journal of Structural Engineering. ASCE; 7: 151. (1961)
[53] Rockey K., Evans H., Porter D. A design method for predicting the collapse behaviour of plate girders. Proceedings of Institution of Civil Engineers. 65 (2): 85-112. (1978)
[54] Höglund T. Shear buckling resistance of steel and aluminium plate girders. Thin-Walled Structures. 29(1-4): 13-30 (1998)
[55] European Committee for Standardization Eurocode 3. EN 1993-1-5. Eurocode 3: desig of steel structures – part. 1.5: plated structural elements. CEN; (2006)
[56] Estrada I., Real E., Mirambell E. General behaviour and effect of rigid and non-rigid end post in stainless steel plate girders loaded in shear. Part II: extended numerical study and design proposal. Journal of Constructional Steel Research. 63(7), 985-996. (2007)
[57] Di Sarno L, Elnashai AS, Nethercot DA. Seismic performance of stainless steel frames. Journal of Constructional Steel Research. 59 (10): 1289–319. (2003)
[58] DiSarno L., Elnashai A., Nethercot D., Seismic response of stainless steel braced frames. J. Constr. Steel Res., 64 (7–8), 914–925, (2008)
[59] Chacón R., Arrayago I., Mirambell E., Real E. Cyclic loading in stainless steel links under lateral loads. Proceedings of Eurosteel. Copenhaguen (2017)
[60] Chacón R., de Marco M., Real E. Arrayago I. An experimental study on the cyclic response of austenitic stainless steel. Ninth International Conference in Steel Structures (ICASS2018). Hong Kong, (2018)
[61] Zhou F., Fang F., Chen Y. Experimental and numerical studies on stainless steel tubular members under axial cyclic loading. Engineering Structures. Vol. 171 (9): 72-85. (2018)

[62] Vega A. Stainless Steel links for eccentrically braced frames. Master Thesis. School of Civil Engineering. https://upcommons.upc.edu/handle/2117/119679 (2018).
[63] Abaqus. Simulia. Dassault Systèmes. V. 6.17. (2017)
[64] Richards P. Uang C., Effect of flange width-thickness ratio on eccentrically braced frames link cyclic rotation capacity. J. Struct. Eng., 131 (10), 1546–1552, (2005).
[65] Yuan H., Wang Y., Shi Y., Gardner L., Residual stress distributions in welded stainless steel sections. Thin-Walled Structures, 79, 38–51, (2014).